Available online www.jsaer.com

***Journal of Scientific and Engineering Research*, 2022, 9(7):105-115**

Research Article

ISSN: 2394-2630
CODEN(USA): JSERBR

Interpretation of the gravity anomaly map of the Sivas (Dumluca) - Turkey iron ore using the Random Neural Network (RNN) method

Ali Muhittin Albora

Istanbul University-Cerrahpaşa, Engineering Faculty, Geophysical Department, 34850, Büyükçekmece-Istanbul, Turkey Email: muhittin@istanbul.edu.tr

Abstract In this paper, Random Neural Network (RNN) has been applied to magnetic map for separation of residual and regional anomalies. It is shown that RNN is the appropriate approach for the prior real-time model since it can perfectly specify the local properties of regions. Additional domain-dependent prior knowledge, such as the sizes, the shapes, the depth and the orientations of regions can be reflected in the parameters of a RNN model. RNN approach has been applied to various synthetic examples. The RNN method was applied to the bouguer anomaly map obtained in the Dumluca iron mine area of Sivas region in Turkey. The resulting anomalies were then compared with the drilling data and successful results were obtained.

Keywords Random Neural Network (RNN), Iron Ore, Bouguer anomaly map, Sivas-Turkey

Introduction

The Bouguer anomaly map obtained from the gravity survey conducted by MTA in the Dumluca mining area of Sivas province Divriği region was used as a field study. Many researchers have worked and are working in the Sivas-Divriği region until today. Some of these researchers [1, 2 ,3]. By applying the RNN method to the Bouguer anomaly map, the residual structure was revealed and the places with a high probability of being a mine were determined. Again, it was checked with the drilling data of Dumluca iron field obtained from MTA and a good overlap was achieved. In this paper, RNN to bouguer anomaly maps is used to separate residual and regional anomalies. It has been shown to be the appropriate approach for the previous real-time model, as RNN can perfectly determine the local characteristics of regions. Additional field-dependent preliminary information, such as dimensions, shapes, depth, and orientation of regions, can be reflected in the parameters of an RNN model. The RNN approach has been applied to various synthetic samples. The RNN method has been used in many studies such as noise analysis and separation methods in geophysical studies [4, 5].

Random Neural Network Approach

Random Neural Network (RNN) model have defined in 1989 and extended and generalized in 1990 by [6,7]. In RNN model, there are positive and negative signals. These signals which are in the form of spikes of unit amplitude circulate among the neurons. Positive signals represent excitation and negative signals represent inhibition. These signals can arrive either from other neurons or from outside world. They are summed at the input of each neuron and constitute its signal potential. Each neuron's state is a non-negative integer number called its potential, which increases when an excitation signal arrives to it, and decreases when an inhibition signal arrives. Thus, an excitatory spike is interpreted as a ``+1" signal at a receiving neuron, while an inhibitory spike is interpreted as a ``-1" signal. If neuron potential is positive, it fires and sends out signals to the other

neurons of the network or outside world. Neural potential also decreases when the neuron fires. Thus a neuron emitting a spike, whether it be an excitation or an inhibition, will lose potential of one unit, going from some state to previous state .

The state of the *n*-neuron network at time *t*, is represented by the vector of non-negative integers $k(t) = (k_1(t),..., k_n(t))$, where $k_i(t)$ is the potential or integer state of neuron *i*. Arbitrary values of the state vector and of the *i*-th neuron's state are shown by k and k_i. Neuron *i* fires (i.e. become excited and send out spikes) if its potential is *positive*. The spikes are sent out at a rate *r*(*i*), with independent, identically and exponentially distributed inter-spike intervals. Spikes go out to some neuron *j* with probability $p^+(i,j)$ as excitatory signals, or with probability $p^-(i,j)$as inhibitory signals. A neuron may also send signals out of the network with probability *d*(*i*). There is a relationship between these probabilities as follows;

$$d(i) + \sum \left[p^+(i,j) + p^-(i,j) \right] = 1 \quad (1)$$

If we show weights between neurons with ω^+ and ω^-, they calculate as follows;

$$\omega^+_{ij} = r(i)p^+(i,j), \quad \omega^-_{ij} = r(i)p^-(i,j) \quad (2)$$

These ω's similar to synaptic weights in connectionist models. Exogenous (i.e. those coming from the ``outside world'') excitatory and inhibitory signals also arrive to neuron *i* at rates $\Lambda(i)$, $\lambda(i)$, respectively. This is a ``recurrent network'' model, *i.e.* a network which is allowed to have feedback loops, of arbitrary topology.

Computations related to this model are based on the probability distribution of network state $p(k,t) = \Pr[k(t) = k]$, or with the marginal probability that neuron *i* is excited $q_i(t) = \Pr[k_i(t) > 0]$.

As a consequence, the time-dependent behavior of the model is described by an infinite system of *Chapman-Kolmogorov* equations for discrete state-space continuous Markovian systems.

Information in this model is carried by the *frequency* at which spikes travel. Thus, neuron *j*, if it is excited, will send spikes to neuron *i* at a frequency $\omega_{ij} = \omega_{ij}^+ + \omega_{ij}^-$. These spikes will be emitted at exponentially distributed random intervals. In turn, each neuron behaves as a non-linear *frequency demodulator* since it transforms the incoming excitatory and inhibitory spike trains' rates into an ``amplitude'', which is $q_i(t)$ the probability that neuron *i* is excited at time *t*. Intuitively speaking, each neuron of this model is also a frequency modulator, since neuron *i* sends out excitatory and inhibitory spikes at rates (or frequencies) $q_i(t)r(i)p^+(i,j)$, $q_i(t)r(i)p^-(i,j)$ to any neuron *j*.

The stationary probability distribution associated with the model is the quantity used throughout the computations:

$$p(k) = \lim_{t\to\infty} p(k,t), \; q_i = \lim_{t\to\infty} q_i(t), \; i = 1,2,..,n \quad (3)$$

It is given by the following result:

Theorem 1. *Let q_i denote the quantity*

$$q_i = \lambda^+(i)/[r(i) + \lambda^-(i)] \quad (4)$$

where the $\lambda^+(i), \lambda^-(i)$ for *i = 1,...,n* satisfy the system of nonlinear simultaneous equations:

$$\lambda^+(i) = \sum_j q_j r(j) p^+(i,j) + \Lambda(i), \quad \lambda^-(i) = \sum_j q_j r(j) p^-(i,j) + \lambda(i) \quad (5)$$

Let *k(t)* be the vector of neuron potentials at time *t* and *k=(k1, ... , kn)* be a particular value of the vector; let *p(k)* denote the stationary probability distribution;

$$p(k) = \lim_{t\to\infty} \Pr[k(t) = k]$$

If a nonnegative solution $\{\lambda^+(i), \lambda^-(i)\}$ exists to equations (4) and (5) such that each $q_i<1$, then

$$p(k) = \prod_{i=1}^{n} [1-q_i] q_i^{ki} \tag{6}$$

The quantities which are most useful for computational purposes, *i.e.* the probabilities that each neuron is excited, are directly obtained from:

$$\lim_{t\to\infty} \Pr[k_i(t) > 0] = q_i = \lambda^+(i)/[r(i) + \lambda^-(i)] \quad \text{if} \quad q_i<1. \tag{7}$$

For notational convenience following is written;

$$\omega^+(j,i) = r(i)p^+(i,j) \geq 0, \quad \omega^-(j,i) = r(i)p^-(i,j) \geq 0$$

$$N(i) = \sum_j q_j \omega^+(j,i) + \Lambda(i), \tag{8}$$

$$D(i) = r(i) + \sum_j q_j \omega^-(j,i) + \lambda(i)$$

Then equation 4 becomes

$$q_i = \frac{N(i)}{D(i)} \tag{9}$$

and

$$r(i) = \sum_j \left[\omega^-(j,i) + \omega^+(j,i)\right]. \tag{10}$$

We can represent this neural network model as shown Figure 1. Actually there isn't any different from other network. Different things that there are two weights between two neurons (ω^+, ω^-). Unless neuron potential is positive, neuron doesn't join to calculate.

Thus this network model similar to a type of genetic algorithm Figure 2.

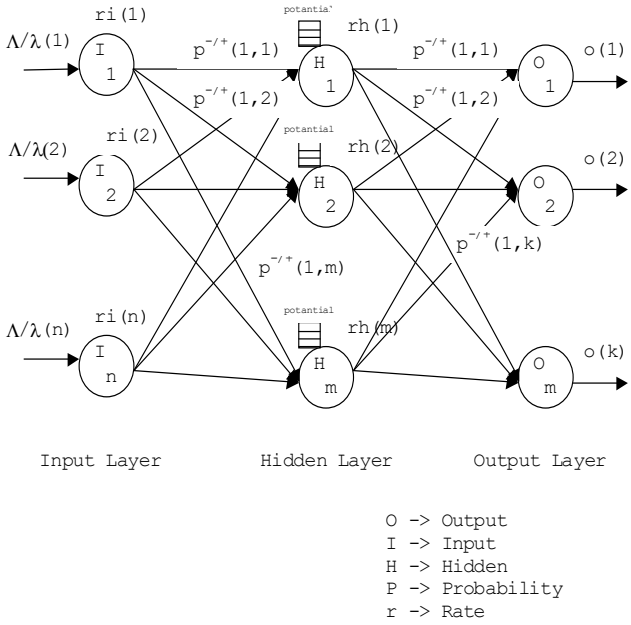

Figure 1: Representation of RNN Model

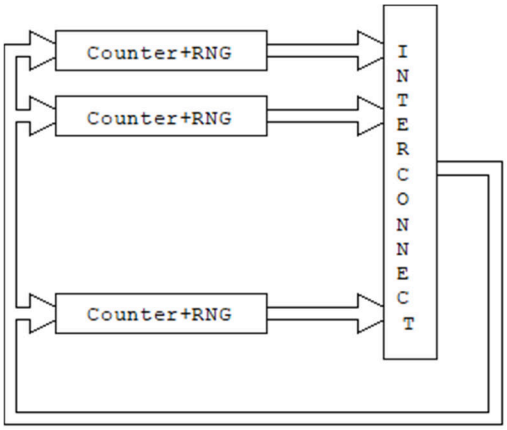

Figure 2: Hardware implementation of the random neuron network model

In addition to RNN can be implemented in hardware as shown in Figure 3. Each neuron is represented by a counter and a Random Number Generator (RNG). To simulate the exponential delays associated with the signal emission, RNG is used. The interconnection network receives signals from counter+RNG represents each neuron. Signals can be viewed as short packets of data containning the signal's polarity and its destination. And interconnection network routes the signal to the apropriate output line to the neuron to which it is adressed.

The Learning Algorithm

Learning algorithm of RNN is based on the algorithm described in (Gelenbe 93). The algorithm chooses the set of network parameters (ω^+, ω^-) in order to learn a given set of K input-output pairs (i, **Y**) where the set of successive inputs is denoted , $i = \{i_1, ..., i_k\}$ and $i_k = (\Lambda_k, \lambda_k)$ are pairs of positive and negative signal flow rates entering each neuron:

$$\Lambda_k = [\Lambda_k(1), ..., \Lambda_k(n)], \qquad \lambda_k = [\lambda_k(1), ..., \lambda_k(n)] \tag{11}$$

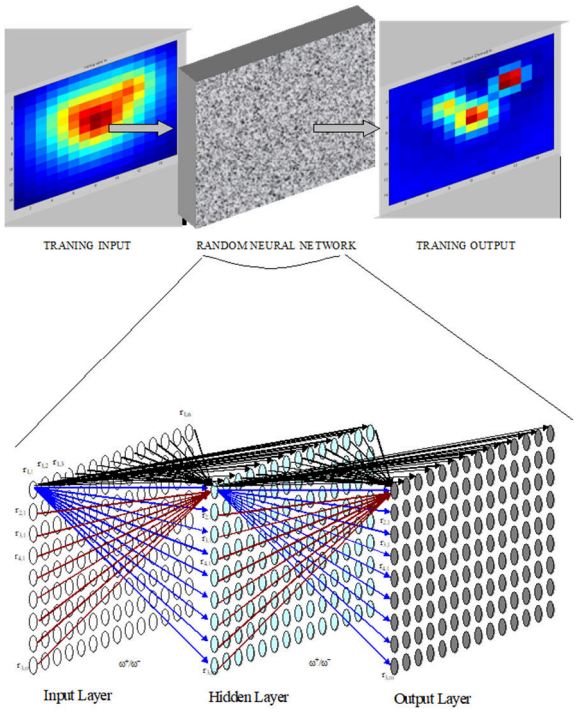

Figure 3: D Representation of RNN Procedure

The successive desired outputs are the vectors , where each vector , whose elements correspond to the desired values of each neuron. The network approximates the set of desired output vectors in a manner that minimizes a cost function :

If we wish to remove some neuron *j* from network output, and hence from the error function, it suffices to set *Both* of the *n* by *n* weight matrices and have to be learned after each input is presented, by computing for each input , a new value and of the weight matrices, using gradient descent. Clearly, we seek only solutions for which all these weights are positive.

Let *w*(*u*,*v*) denote any weight term, which would be either , or . The weights will be updated as follows:

where is some constant, and

1. is calculated using the input and , in Equation 3.
2. is evaluated at the values and .

To compute we turn to the expression 3, from which we derive the following equation:

Let and define the matrix

We can now write the vector equations:

where the elements of the *n*-vectors , are Notice that where denotes the *n* by *n* identity matrix. Hence the main computational work is to obtain This is of time complexity , or if an *m*-step relaxation method is used.

We now have the information to specify the complete learning algorithm for the network. We first initialize the matrices and in some appropriate manner. This initiation will be made at random. Choose a value of , and then for each successive value of *k*, starting with *k* = 1 proceed as follows:

1. Set the input values to .
2. Solve the system of nonlinear equations 3 with these values.
3. Solve the system of linear equations (8) with the results of (2).
4. Using equation 7 and the results of (2) and (3), update the matrices and . Since we seek the ``best'' matrices (in terms of gradient descent of the quadratic cost function) that satisfy the *nonnegativity* constraint, in any step *k* of the algorithm, if the iteration yields a negative value of a term, we have two alternatives:
    1. Set the term to zero, and stop the iteration for this term in this term in this step *k*; in the next stop *k*+1 we will iterate on this term with the same rule starting from its current null value;
    2. Go back to the previous value of the term and iterate with a smaller value of .

This general scheme can be specialized to feedforward networks yielding a computational complexity of , rather than , for each gradient iteration.

Application of the RNN method to synthetic data

Table 1: Model parameters of 3 spheres

Parameter	Birinci Küre	İkinci Küre	Üçüncü Küre
Çap (r)	5	5	7
Yoğunluk (ρ)	3	3	3
Derinlik (h)	3	4	3
X Koordinatı	11	6	8
Y Koordinatı	11	11	8

Sphere models obtained by using Relation-12 were used in the preparation of the synthetic map. For the first synthetic model, 3 spheres with different parameters were taken (Table-1). The input of the Bouguer anomaly map formed by these spheres into Random Neural Networks and the output of the residual anomaly map are shown in Figure-4.

$$G = \frac{k_0 m.h}{(x^2 + y^2 + h^2)^{3/2}} \qquad (12)$$

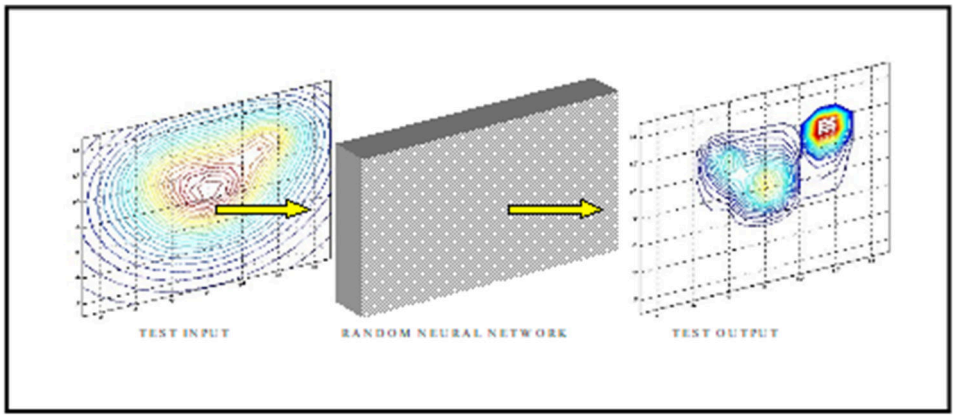

Figure 4: RNN inputs and outputs of the artificially generated Bouguer anomaly map given in Table 1.

Secondly, the given synthetic model was also used 3 spheres with different parameters and is shown in Table-1. In this model, a deep sphere is given and an attempt is made to eliminate the effect of this sphere and remove the residual effect. (Figure-5).

Table 2: Parameters of the synthetically generated Bouguer anomaly map consisting of spheres.

Parameter	K1	K2	K3
Çap (r)	30	4	3
Yoğunluk (ρ)	1.8	1.2	1.3
Derinlik (h)	100	6	5
X Koordinatı	6	5	12
Y Koordinatı	6	5	8

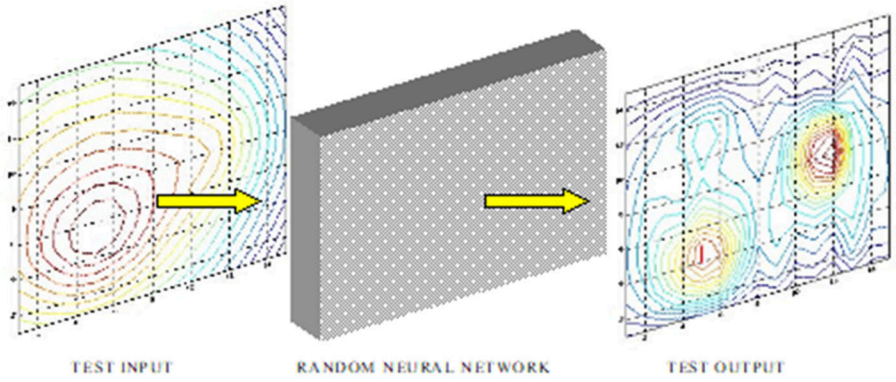

Figure 5: RNN inputs and outputs of the artificially obtained Bouguer anomaly map given in Table 2.

Geology of the region

Dumluca ore field is located in the northwest of Sivas, which is a city in Turkey (Figure 6a). The village of Dumluca is located in the north-western part of the province of Divriği in Sivas province. The region was located in the Tethys geosynclinals region along the Mesozoic. The marine limestone massifs formed in this period indicate this characteristic. The crystal of the geosynclinals base, which is not visible in the study area, should be Paleozoic. This Paleozoic basement has overturned to the north and south of the region. The orozygous development of the Mesozoic completed the Laramiende (Cretaceous end), and the Upper Cretaceous folds ascended to the terrestrial zone from deep-sea facies. The Paleocene kanglomals that come uncomfortably over the Cretaceous folds are in shallow sea character. In fact, these kanglomeralites cannot be distinguished

precisely in the field of study, but are possible to see in the environment. Eocene Tethys is the result of re-flooding the sea, the region is a volatile geosyncline. In this era, it is seen that many regions that have risen so much in Laramie have stayed on the water in the islands. Nummulitic limestone's are formed in the deep parts of the sea and volcanic Eocene flysches are formed in the shallower parts. Eocene is mostly over older formations with a transgression. The Oligocene region is generally shallow marine, with variegated sandstones and sometimes gypsiferous, saline floors. With the effect of radon orogeny developing after the Miocene, both the Miocene folds and the Miocene Sea retreats. After that, in the territory turned into land, large and thick conglomerate floors were formed with a rainy climate effect. These conglomerates formed thick masses in the pits where the ancient Miocene marine was located [8]. The region is located on the east of the Taurus Mountains. A large part of the area contains blocks of various age types and sizes, units belonging to the Bozkir Unit consisting of rocks (allokton) units. These units contain ophiolite blocks, tuffs and basic submarine volcanics of varying sizes.The oldest rock unit in the region is composed of Permian aged, quartzite calcschist, phyllite and dolomitic limestone which are exposed in the vicinity of Bakır Tepe in the north of Alacahan. The Mesozoic in the region is a thick sediment consisting of thick sedimentary carbonates. The granitic rocks did not bring up ore solutions, as they used to be, and they formed the hornfels zones by influencing the side rocks with some liquids and by moving the waters in the side rock by heat effect, they formed beds by moving the demagnetizations in serpentinized basic and ultrabasic rocks (Figure 6b). In Plio-Quaternary tuff, tuffite, anglomera and basalts spread especially around Dumluca [8, 9].

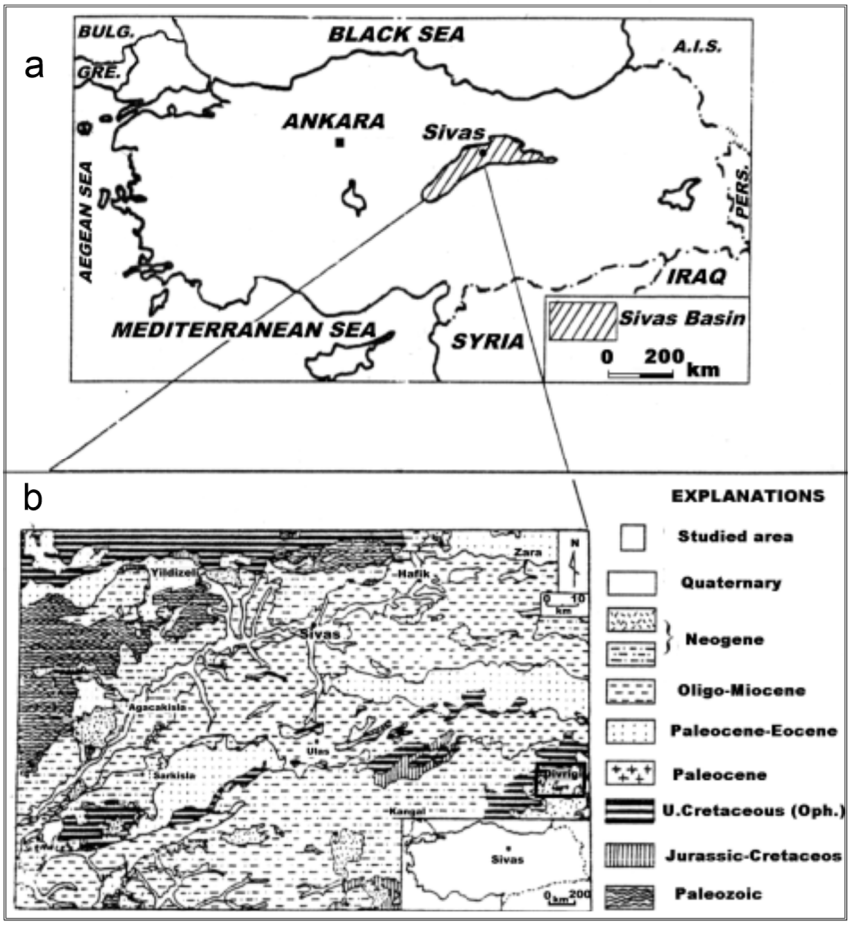

Figure 6: Working area a) Turkey-Sivas Dumluca iron ore b) Geology of the region [8, 9].

The serpentinized basic and ultra-basic rocks form the source of iron ores in the region. Granitic rocks have not brought out ore solids as we once thought. The hornfels zones formed by influencing the side rocks with some

liquids and the waters in the side rocks were serpentinized by the effect of heat again. The debris in the basic and ultrabasic rocks keeps the beds from moving. In Plio-Quaternary tuff, tuffite, anglomera and basalts spread around Dumluca (Figure 6) [8, 9].

The Dumluca iron deposit is located at the contacts of plutonic rocks intruded by lamprophyre dikes. Field geology indicates the covering layer consists of basalt and conglomerate. The associated rocks are serpentines and granites. The iron ore, randomly distributed within the serpentine, is generally magnetite and rarely hematite. The upper part of magnetite was altered to martite, but the lower part remained as massive (not altered). We note that the iron region contains pyrite and occasionally serpentine intercalation. The region is located east of Toros Mountain of Turkey. It is covered by blocks and allochtonous units (Figure 7).

In the Dumluca iron ore region, D-1 and D-2 were the first drillings. Afterwards, D-4, D-6, D-7, D-9, D-10, D-13, D-14A, D-14, D-18, D20 and D24 drillings were executed (Yildiz 1977). In D-9 and D-18, no iron was detected, but elsewhere, in other drillings, iron ore was found at different depths (Figure 8).

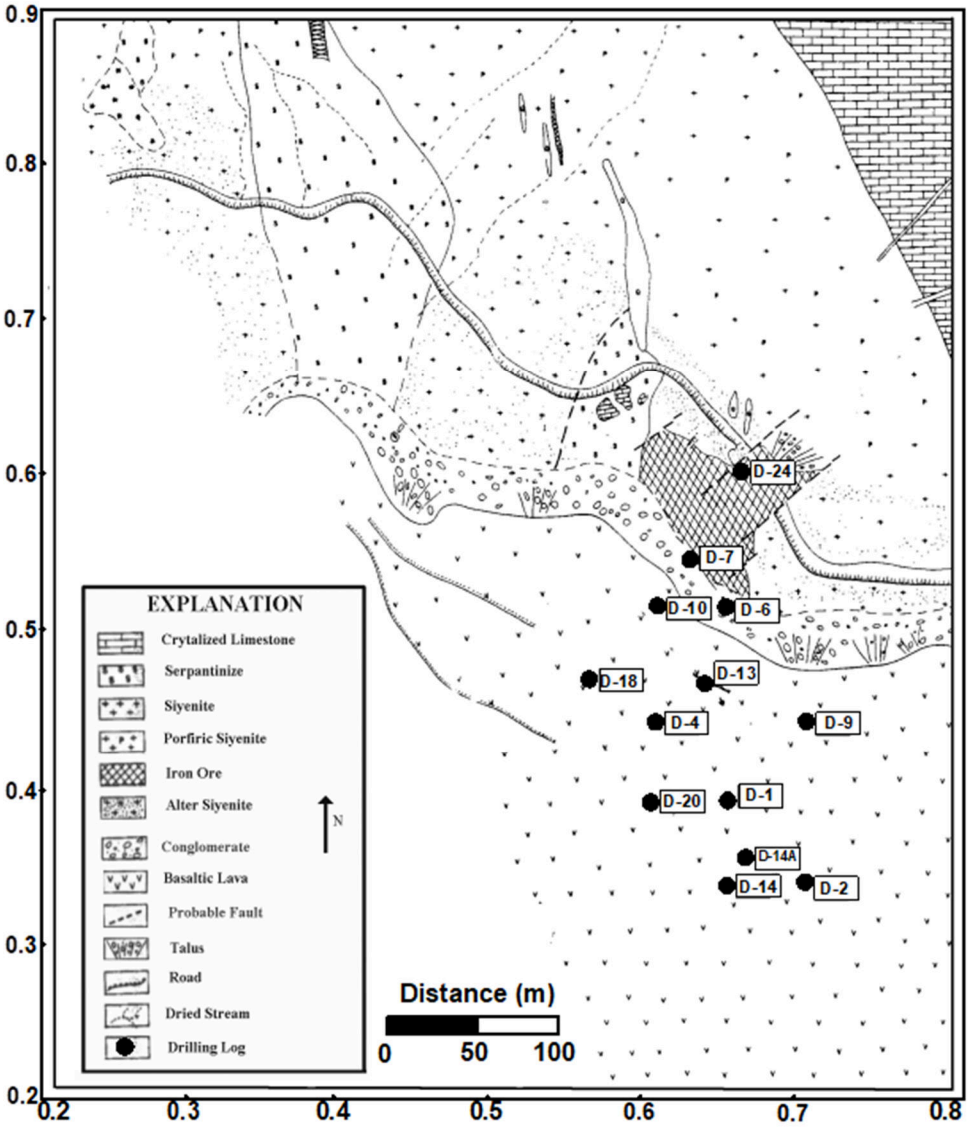

Figure 7: Geological map of Dumluca region [9, 10]

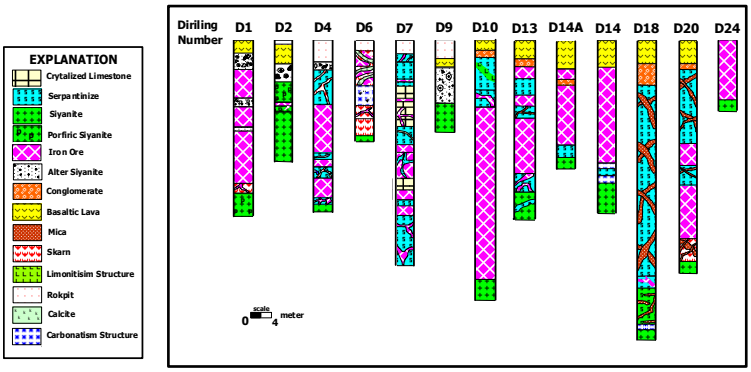

Figure 8: Drilling Logs of the Dumluca iron ore reserves [8, 9, 10]

Geophysical studies in the region

A map of gravity anomaly was obtained by the Mineral Research and Exploration Institute (MTA) at Dumluca mine site (Figure 9). When looking at the Bouguer anomaly map, two different anomalous sites are visible. Anomaly values increase as the center approaches east. The Dumluca Bouguer anomaly map continues with an increase of 5.6 mgal toward the center, starting at 2.4 mgal. On the Bouguer anomaly map, drilling locations are also shown. The RNN method was applied to the Bouguer anomaly map (Figure 10).

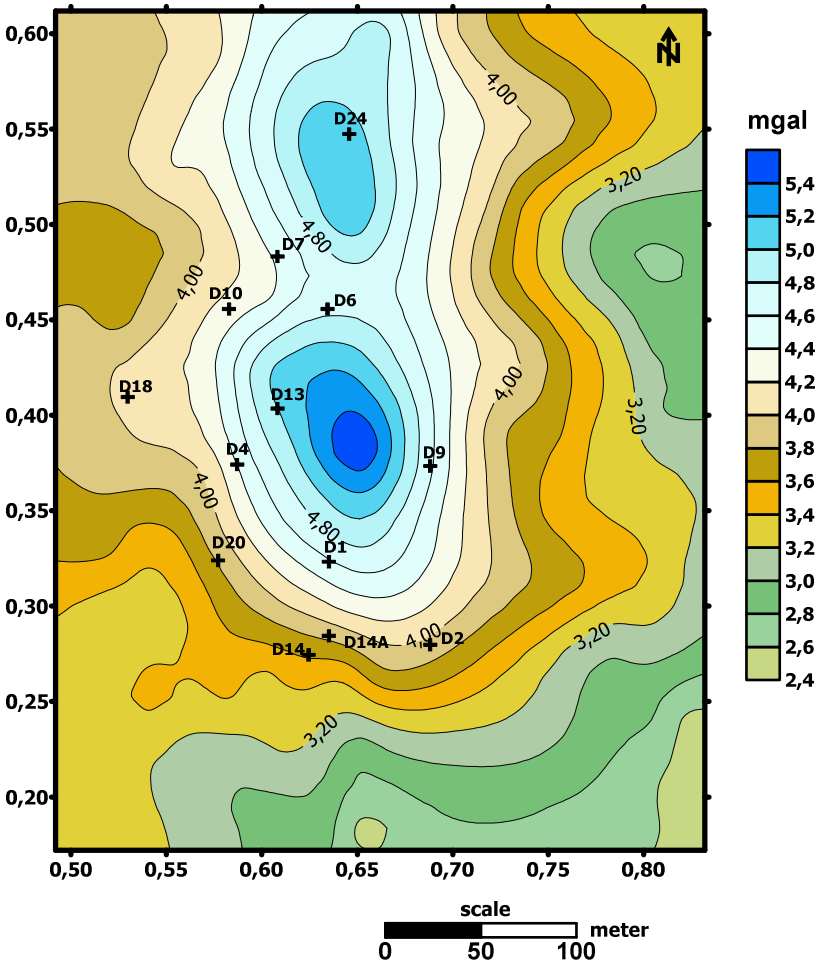

Figure 9: Gravity anomaly map of Dumluca iron ore area (contour interval is 0.2 mGal).

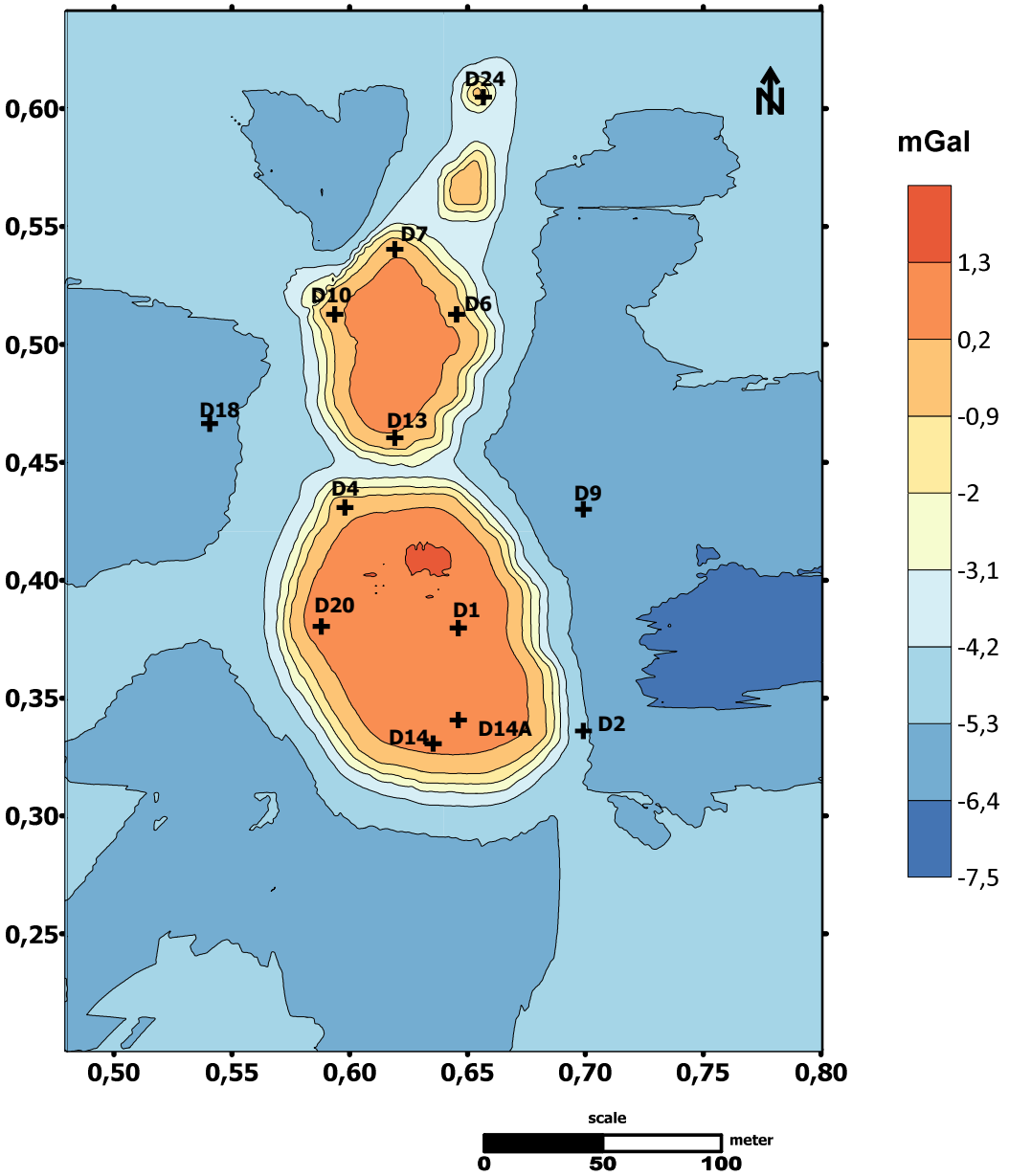

Figure 10: RNN output of the Dumluca mine site gravity anomaly map

Results and Discussion

When looking at the RNN output of the Bouguer anomaly map, no anomaly was observed in the D-2 and D-9 drilling areas, and no metal was found in the drillings (Figure 8). Although there is no anomaly at the CNN exit of the site where the D-18 borehole is located, it appears that the basaltic lava in this place is caused by the effect of canglomerate. The anomaly effect is also observed in the place where the D-24 bore is located, and this location is very close to the surface of the mine. D-14 and D14A are located just below the mine basalt lava in the drilling sites.The thickness of the cover of Pliocene conglomerate and basalts above the ore level in the Dumluca iron bed is low. The thickness of this veil covering most of the bed is 20-30 m. between. Only the D-18 sounding goes beyond the fact that the bed is plunging to the west. In D-20 sounding this thickness is 80 m. 54 m in D-4. 40 m in D-10.

Acknowledgement
This research was supported by Research Institute of Istanbul University (The Project Number: 1247/050599). The authors wish to thank MTA for providing of potential field data for this study.

References

[1]. Dogan, H., Yildizeli, N., Yurt, M.Z., Celebi, A. & Ozcan, H (1989). T.D.C.I. Genel Müdürlüğü adına, Sivas Divriği Çevresinde II-59, AR: 33613- Poligon-II. IR: 922 ruhsat alanlarında yapılan demir etüdü jeoloji raporu, M.T.A Gen.Mud, 89/120, Ankara.
[2]. Önder, E., & Yildizeli, N (1985). Sivas-Divrigi Akdag demir yatagı jeoloji raporu, M.T.A, Ankara.
[3]. Üçer, A (1999). Dumluca (Divriği) Sahasının Yorumlanması, İstanbul Universitesi Fen Bilimleri Enstitusü Doktora tezi.
[4]. Albora, A. M (2020). Image Processing on Ruins of Hitite Civilization Using Random Neural Network Approach. *Journal of Scientific and Engineering Research*, 7(3):196-205
[5]. Danacı, E., Uçan O. M., & Albora A. M (2000). Gravite anomali haritalarına yeni bir yaklaşım: Rastgele Yapay Sinir Ağları Uygulamalı Yerbilimleri- , cilt.1, sa.6, ss.61-68, 2000
[6]. Gelenbe, E (1989). Random Neural Networks with Negative and Positive Signals and Product Form Solution, Neural Computation, **1**, 4, 502-511.
[7]. Gelenbe, E (1990). Stability of The Random Neural Network Model. Neural Computation, **2**, 2, 239-247.
[8]. Öztürk, H (1991). Divrigi ore province and source comments: Ph.D. Thesis, Istanbul University, Science and Technology Institute.
[9]. Albora, A. M., Ucan, O. N (2006) "Separation of Magnetic Field Data Using Differential Markov Random Field (DMRF) Approach", Geophysics, 71, 125-134.
[10]. Yıldız, N. (1977). Drilling Report of Divrigi-Dumluca Iron Ore, MTA Report No. 315, Ankara.